

# A biophysical signature of network affiliation and sensory processing in mitral cells

Kamilla Angelo<sup>1,2</sup>, Ede A. Rancz<sup>1,3</sup>, Diogo Pimentel<sup>1</sup>, Christian Hundahl<sup>2,4</sup>, Jens Hannibal<sup>4</sup>, Alexander Fleischmann<sup>5</sup>, Bruno Pichler<sup>3</sup> & Troy W. Margrie<sup>1,3</sup>

**One defining characteristic of the mammalian brain is its neuronal diversity<sup>1</sup>. For a given region, substructure, layer or even cell type, variability in neuronal morphology and connectivity persists<sup>2–5</sup>. Although it is well known that such cellular properties vary considerably according to neuronal type, the substantial biophysical diversity of neurons of the same morphological class is typically averaged out and ignored. Here we show that the amplitude of hyperpolarization-evoked sag of membrane potential recorded in olfactory bulb mitral cells is an emergent, homotypic property of local networks and sensory information processing. Simultaneous whole-cell recordings from pairs of cells show that the amount of hyperpolarization-evoked sag potential and current ( $I_h$ )<sup>6</sup> is stereotypic for mitral cells belonging to the same glomerular circuit. This is corroborated by a mosaic, glomerulus-based pattern of expression of the HCN2 (hyperpolarization-activated cyclic nucleotide-gated channel 2) subunit of the  $I_h$  channel. Furthermore, inter-glomerular differences in both membrane potential sag and HCN2 protein are diminished when sensory input to glomeruli is genetically and globally altered so that only one type of odorant receptor is universally expressed<sup>7</sup>. Population diversity in this intrinsic property therefore reflects differential expression between local mitral cell networks processing distinct odour-related information.**

Neurons show a broad array of biophysical properties that profoundly impact the computations that they perform. Even within cell types, diversity in morphology<sup>8</sup>, and expression of molecular markers<sup>1</sup> and ion channels<sup>9</sup> is well documented, but whether such variation reflects necessary biological noise<sup>10</sup> or perhaps a functional, dynamic system for regulating excitability at the cellular<sup>11</sup> or even network level remains unclear. The hyperpolarization-activated current ( $I_h$ ; also observed as a sag potential) is one intrinsic biophysical property that is known to influence the input–output function<sup>12–17</sup> of most principal cell types<sup>18</sup>. In the olfactory bulb, the broad amplitude distribution of  $I_h$ -mediated sag potential recorded across the mitral cell population has recently been shown to reflect functional diversity in their input–output responses to *in vivo* stimuli<sup>6</sup>.

To explore directly whether cell-to-cell variability in membrane potential sag might reflect differences between functional ensembles of mitral cells, we have taken advantage of the fact that in some brain regions the local architecture facilitates the identification of functionally discrete networks of neurons<sup>19</sup>. This is particularly true for the olfactory bulb, where glomeruli act as information hubs that receive inputs from a unique, homogeneous population of sensory afferents<sup>20</sup> that are integrated by a network of a few hundred interconnected local interneurons and principal mitral and tufted cells. Thus, in a slice preparation, individual mitral cells can be precisely linked to the functional circuit in which they operate *in vivo*<sup>21,22</sup>, permitting us to explore whether their intrinsic diversity reflects an emergent property of the functional organization of the olfactory bulb (Fig. 1A).

In wild-type mice, mitral cells can exhibit a hyperpolarization-evoked rebound potential and current indicative of the  $I_h$ -mediated sag potential recently described in the rat, both *in vitro* and *in vivo*<sup>6</sup> (Supplementary Fig. 1). The distribution of sag potential amplitude (SPA) recorded across the mitral cell population in mouse is similarly uni-modal ( $P < 0.05$ ) and broad (min = –10.4 mV, max = 30.65 mV, median = 3 mV, mean =  $3.43 \pm 5.8$  mV,  $n = 105$  cells,  $n = 39$  animals; Fig. 1B and Supplementary Fig. 1). To explore the possibility that such population diversity might reflect differences between local mitral cell networks (Fig. 1A), we performed simultaneous whole-cell recordings of sag from pairs of cells belonging to distinctly different (Fig. 1C, a) or the same glomerular ensemble (Fig. 1C, b). The mean SPA found under these two recording scenarios was not significantly different (inter-glomerular pairs,  $3.3 \pm 6.7$  mV,  $n = 52$  cells versus intra-glomerular pairs,  $2.45 \pm 3.72$  mV,  $n = 28$  cells ( $P = 0.41$ ); Fig. 1D). For each recorded pair we determined the absolute difference in SPA (Supplementary Fig. 2) and performed a multiple pair-wise comparison, whereby the SPA difference between each cell and all other cells within the same group—excluding its simultaneously recorded ‘partner’—was calculated (‘pseudo pairs’, Fig. 1E). For inter-glomerular pairs of mitral cells, the distribution of SPA difference between recorded and pseudo pairs was similar (recorded: min = 0.03 mV, max = 21.06 mV, median = 3.57 mV, Q1 = 1.87 mV, Q3 = 5.35 mV,  $n = 26$  pairs, versus pseudo pairs: min = 0.01 mV, max = 41.05 mV, median = 4.435 mV, Q1 = 1.78 mV, Q3 = 9.46 mV,  $n = 1300$  ( $P = 0.16$ ); Fig. 1E, F). This was also the case when comparing inter-glomerular recorded pairs and pseudo pairs extracted from our entire data set ( $n = 105$  cells, 5,460 pseudo pairs; Supplementary Fig. 2).

In contrast, the sag potential and the  $I_h$ -current amplitude recorded simultaneously from mitral cells belonging to the same glomerular network were virtually indistinguishable (Supplementary Fig. 2). Thus, the difference in the SPA recorded from intra-glomerular pairs was significantly smaller than that determined for intra-glomerular pseudo pairs (recorded SPA difference for intra-glomerular pairs: min = 0 mV, max = 3.59 mV, median = 1.22 mV, Q1 = 0.31, Q3 = 2.1 mV,  $n = 14$  pairs, versus intra-glomerular pseudo pairs: min = 0 mV, max = 12.75 mV, median = 4.23 mV, Q1 = 1.99, Q3 = 6.41 mV,  $n = 364$  pairs ( $P = 0.00002$ ); Fig. 1E, F and Supplementary Fig. 2), for inter-glomerular recorded pairs ( $P = 0.024$ ; Fig. 1F, G) and pseudo pairs extracted from all cells ( $n = 105$  cells;  $P = 0.00001$ ; Fig. 1F and Supplementary Fig. 2). The broad range of sag and  $I_h$ -current amplitudes recorded across the bulb therefore reflects differences between individual glomerular circuits, in which it is a homotypic feature of the local mitral cell network (Fig. 1G).

Cell-attached experiments in mitral cell apical dendrites indicate that the  $I_h$  current is largest in patches recorded in the very distal region<sup>6</sup>. Thus, the recorded membrane potential sag may reflect activation of HCN channels that are expressed predominantly in the

<sup>1</sup>Department of Neuroscience, Physiology and Pharmacology, University College London, Gower Street, London WC1E 6BT, UK. <sup>2</sup>Department of Neuroscience and Pharmacology, Faculty of Health Sciences, University of Copenhagen, 2200 Copenhagen N, Denmark. <sup>3</sup>Division of Neurophysiology, MRC National Institute for Medical Research, Mill Hill, London NW7 1AA, UK. <sup>4</sup>Department of Clinical Biochemistry, Bispebjerg Hospital; University of Copenhagen, 2200 Copenhagen N, Denmark. <sup>5</sup>Center for Interdisciplinary Research in Biology (CIRB), Collège de France, 11 Place Marcelin Berthelot, 75231 Paris Cedex 05, France.

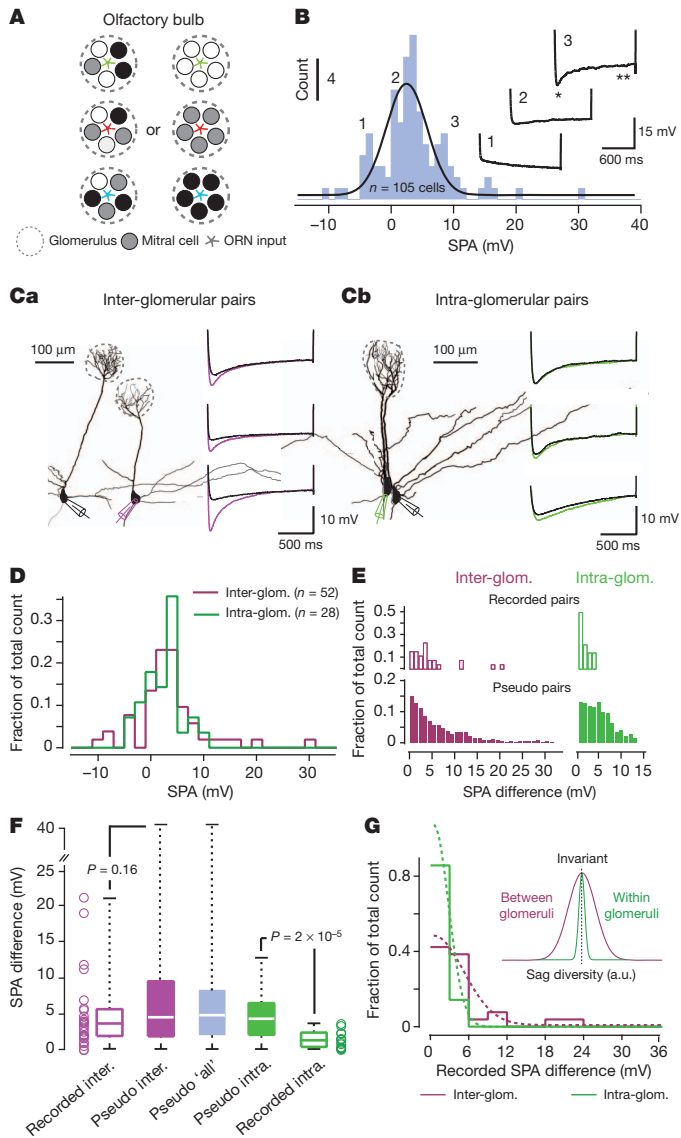


**Figure 1 | Diversity of sag potential amplitude within and between mitral cell networks.** **A**, Schematic of two possible scenarios underlying the population diversity of mitral cell sag. Each olfactory glomerulus receives genetically unique input (shown in red, green and blue). Membrane potential sag (shown by different coloured circles) may be hetero- (left) or homogeneously (right) expressed with the glomerulus. ORN, olfactory receptor nerve. **B**, Histogram (fitted with a Gaussian curve) showing the distribution of SPA recorded across the mitral cell population ( $n = 105$  cells). Traces, three examples recorded from cells belonging to the indicated bins. The sag potential amplitude is determined as the voltage difference between the peak hyperpolarization (shown by an asterisk) and the steady-state membrane potential (shown by two asterisks). **Ca, b**, Example morphologies of two simultaneously recorded mitral cells projecting to either different (**Ca**) or the same (**Cb**) glomerular networks. The voltage traces show the sag potential recorded in three examples of inter- and intra-glomerular pairs. **D**, Histograms of the SPA for all individual cells belonging to either inter- and intra-glomerular pairs. **E**, Top panel, histograms of recorded SPA differences for inter- ( $n = 26$ ) and intra-glomerular ( $n = 14$ ) pairs. Bottom panel, histograms of SPA differences for inter- and intra-glomerular pseudo pairs. **F**, Box-plot of recorded and pseudo inter-glomerular pairs, pseudo pairs of all recordings, and intra-glomerular pseudo and recorded pairs. Open circles, individual data points of recorded SPA difference. **G**, Histogram of sag amplitude difference for inter- and intra-glomerular recorded pairs fitted with a half Gaussian ( $n = 26$  and  $14$  pairs, respectively; bin size,  $3$  mV). Inset, Gaussian fits of the recorded data for intra-glomerular and inter-glomerular pairs. a.u., arbitrary units.

dendritic tuft, the site of sensory integration within the glomerulus. To explore this possibility, we performed immunohistochemical staining for the HCN2 subunit that can form both homomeric or heteromeric HCN channels known to mediate the slow  $I_h$  (ref. 23) underlying mitral cell sag<sup>6</sup>. Qualitatively, very little HCN2 protein was seen in the granule cell and mitral cell layers<sup>24</sup>. In contrast to the low but homogeneous HCN2 expression in the external plexiform layer<sup>24</sup>, we found a high-contrast mosaic staining pattern across the glomerular layer (Fig. 2a). To determine whether HCN2 expression within the glomerulus was postsynaptic to olfactory receptor neuron input we next used a transgenic mouse line that expresses the tau-LacZ transgene in the sensory afferents under the olfactory marker protein (OMP) promoter (OMP-IRES-tau-LacZ mice)<sup>7</sup>. Double-staining experiments against both LacZ and HCN2 showed that the HCN2 protein is predominantly expressed in dendritic compartments within the glomerulus and downstream of the olfactory receptor input (Fig. 2b–d)<sup>25</sup>. Irrespective of the potential contribution of other cell types<sup>24,26</sup>, this mosaic pattern of HCN2 expression is consistent with the observation of large  $I_h$  currents in the distal apical dendrite and the broad range of sag amplitudes recorded in mitral cells participating in different glomerular networks.

Such glomerular-based SPA and HCN2 expression might reflect network-related homeostatic regulation<sup>27,28</sup> of excitability, in which glomerular differences arise from the processing of functionally and

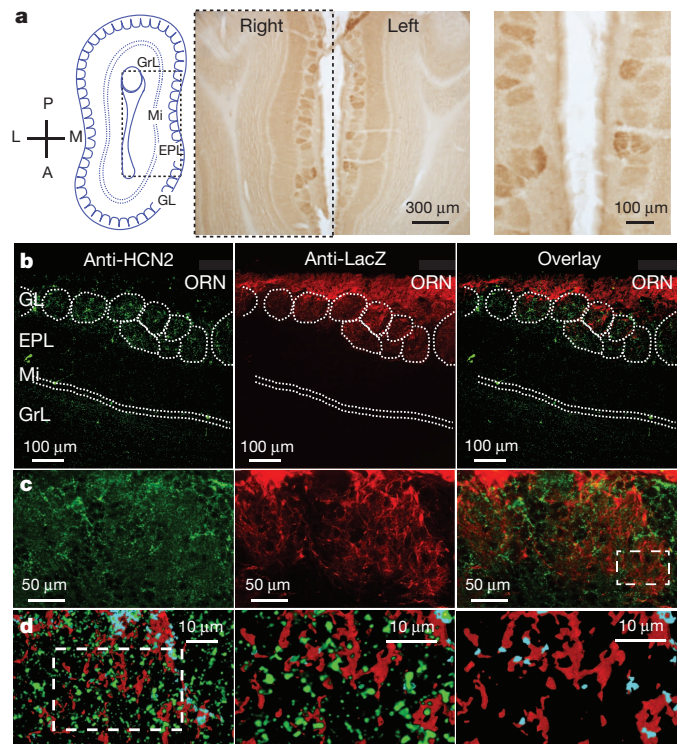


**Figure 2 | Glomerular expression of HCN2 in wild-type and OMP-IRES-tau-LacZ mice.** **a**, Left panel, schematic of a horizontal section of an olfactory bulb highlighting its anatomical organization. A, anterior; L, lateral; M, medial; P, posterior. Middle and right panels, HCN2–DAB staining highlighting glomerular diversity. **b**, Left and middle panels, anti-HCN2 and anti- $\beta$ -galactosidase staining in OMP-IRES-tau-LacZ mice. Right panel, green and red channels shown together for comparison. **c**, High-magnification images of the glomerular layer (colours as in **b**). **d**, Left, higher-magnification images scanned as 30 digital sections, shown as a pseudo three-dimensional image of an approximately  $6\text{-}\mu\text{m}$  thick section. Areas of overlap between green and red are shown in light blue and indicate close proximity of the HCN2 and OMP-LacZ signals. Middle and right panels, images of the outlined area shown in the left panel (anti-HCN2 staining (green colour) has been removed for clarity). EPL, external-plexiform layer; GL, glomerular layer; GrL, granule-cell layer; Mi, mitral cell layer; ORN, olfactory receptor nerve layer.

genetically unique subsets of olfactory input<sup>20</sup>. To test this hypothesis we next performed experiments in a transgenic ‘monoclonal nose’ mouse that expresses the M71 odorant receptor in more than 95% of receptor neurons<sup>7</sup> (M71tg mice, Fig. 3A). We calculated mean pixel intensities of glomeruli in HCN2–DAB-stained M71tg and control animals that revealed significantly different variances ( $P = 0.001$ ) whereby the mean pixel intensity for glomeruli varied less in the M71tg mice than in the control mice ( $P = 0.0025$ ; Fig. 3A, Supplementary Fig. 3). Simultaneous recordings from inter-glomerular pairs of mitral cells in M71tg mice (min = 0.08 mV, max = 6.3 mV, median = 3.3 mV, Q1 = 1.32 mV, Q3 = 3.78 mV;  $n = 24$ ; Fig. 3B, a) also revealed a significantly narrower distribution of SPA difference compared to wild-type and control mice (min = 0.23 mV, max = 21.04 mV, median = 3.4 mV, Q1 = 1.78 mV, Q3 = 10.78 mV,  $n = 24$  ( $P = 0.004$ ); Fig. 3B, a and b, C). This reduction in sag amplitude diversity was also notable for pseudo-pair comparisons for all recorded pairs (Fig. 3D, a) and the overall population data set (M71tg mice: min = 0 mV, max = 36.01 mV, median = 3.4 mV, Q1 = 1.6, Q3 = 6.1 mV,  $n = 91$  cells, 4,095 comparisons, versus M71 control mice: min = 0 mV, max = 51.4 mV, median = 4.6 mV, Q1 = 2, Q3 = 10.19 mV,  $n = 81$  cells, 3,321 comparisons ( $P < 4 \times 10^{-47}$ ); Fig. 3D, a and c). Thus, mitral cells and glomeruli in M71tg mice are more homogeneous in their sag and HCN2 expression profile than those in wild-type and M71 control mice receiving the normal, genetically diverse, array of olfactory receptor neuron input.

Despite the overall reduction in SPA variance in the M71tg mice, the SPA in the intra-glomerular pairs remained more similar (M71tg intra-glomerular pairs: min = 0.2 mV, max = 6.5 mV, median = 0.8 mV, Q1 = 0.3 mV, Q3 = 1.26 mV;  $n = 9$ , versus M71tg inter-glomerular pairs ( $P = 0.04$ ); Figs 3C and 4a). Indeed, we observed no effect of wholesale expression of the M71 receptor on intra-glomerular sag diversity (M71tg versus control and wild-type mice;  $P = 0.61$  and 0.46, respectively; Fig. 4a). Thus, sensory afferent input seems unlikely to be the sole driver of inter-glomerular diversity (Fig. 4b).

Using the hyperpolarization-evoked sag potential as a general proxy, we have identified several organizing principles regarding the population diversity of  $I_h$  expression in mitral cells<sup>6,29</sup>. First, this intrinsic property is a biophysical fingerprint of local constellations of mitral cells forming a functionally discrete olfactory network (Fig. 4c). As mitral cells are electrically and exclusively coupled to their intra-glomerular counterparts, co-regulation of the  $I_h$  channel and current via gap junctions may contribute to their biophysical similarity<sup>9</sup>. Second, analysis of the M71tg mouse shows directly that this network-affiliation-based signature depends on sensory information processing. The fact that in the M71tg mouse intra-glomerular sag diversity remained more homogeneous than in the overall population also suggests that other factors such as feed-forward and lateral inhibition may contribute to sag regulation at the level of the glomerulus. From a functional perspective, mitral cell  $F-I$  curves (frequency of spiking output of neurons ( $F$ ) in response to varying current injection

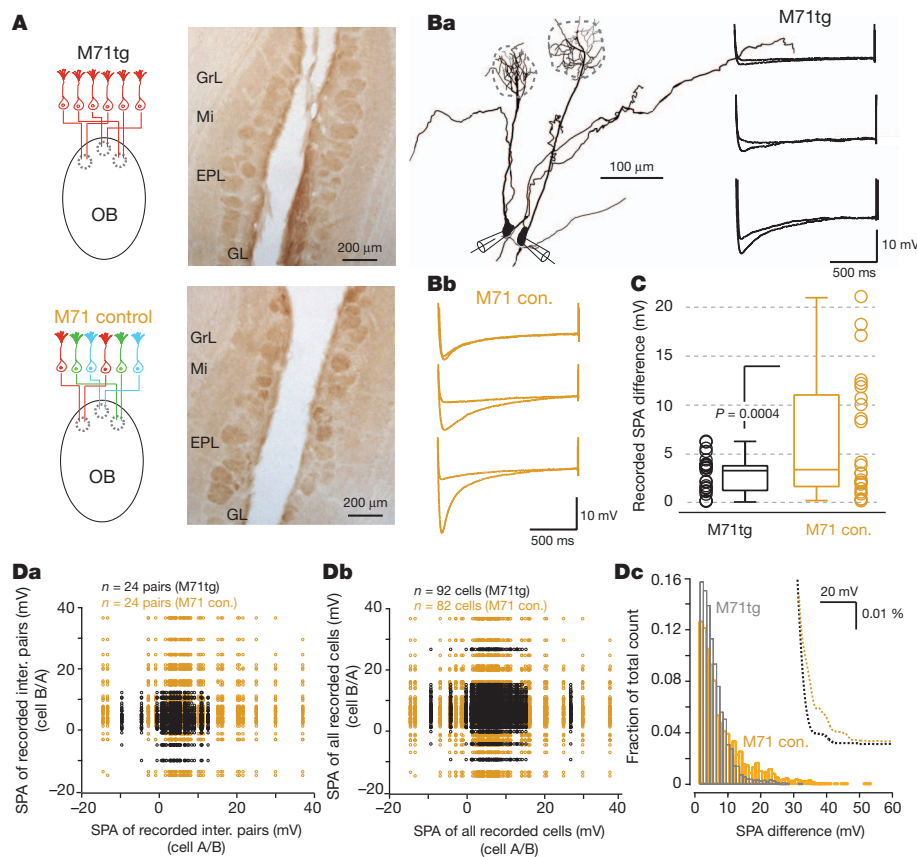


**Figure 3 | Glomerular expression of HCN2 and mitral cell sag in M71 monoclonal mice.** **A**, Schematics of the genetic organization of the nose to brain connectivity in M71tg and control mice (left panels). In contrast to the normal genetically diverse ORNs and glomerulus-specific projection pattern in wild-type and control animals, the sensory afferents to all glomeruli in the transgenic mice express the same M71 receptor (red). HCN2–DAB staining (right panels) in horizontal olfactory bulb (OB) slices from an M71tg mouse and a M71 control mouse. **Ba, b**, Example morphologies of two simultaneously recorded mitral cells belonging to distinctly different glomeruli (inter-glomerular pair) in the M71 transgenic mouse. The voltage traces show

the sag potential recorded in three different example pairs in M71tg (**Ba**) and control mice (**Bb**). **C**, Box-plot of the SPA difference for inter-glomerular recorded pairs from M71tg and control mice. Open circles, individual data points of recorded SPA difference. **Da, b**, Scatter-plots of SPA for pseudo pairs from paired inter-glomerular recordings in the M71tg and control mice. **Dc**, Histogram of SPA differences for pseudo pairs extracted from all cells recorded in the M71tg ( $n = 91$  cells, 4,095 comparisons) and control mice ( $n = 81$  cells, 3,321 comparisons; bin size, 1 mV). Inset, histogram spline fits are overlaid and zoomed in to highlight the disparity between the distributions.

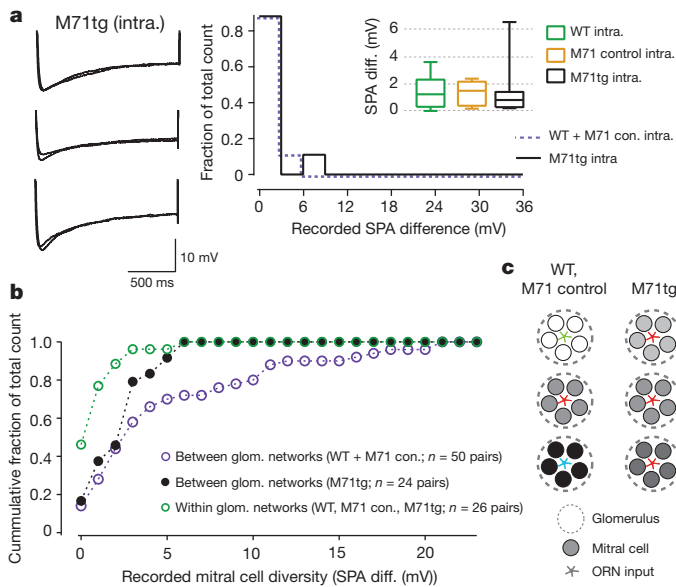


**Figure 4 | Population diversity reflects local network membership and sensory processing.** **a**, Left, example membrane-voltage traces showing the sag potential recorded in three different intra-glomerular pairs from the M71tg mouse. Right, histogram of the SPA difference recorded for intra-glomerular pairs in M71tg mice ( $n = 9$  pairs) versus M71 control and wild-type (WT) mice (pooled:  $n = 17$  pairs). Inset, box-plot of SPA difference for intra-glomerular pairs recorded in wild-type ( $n = 14$ ), M71 control ( $n = 3$ ) and M71tg ( $n = 9$ ) mice. **b**, Summary data plotted as a cumulative histogram of SPA difference of all recorded pairs. **c**, Schematic highlighting the relationship between glomerulus affiliation, sensory input and mitral cell sag diversity.

amplitudes ( $I$ ) are known to shift left, from a sigmoid towards a linear operation with increasing sag<sup>6</sup>. We suggest that the glomerular basis of this delineation may therefore reflect a network-based gain control mechanism and contribute to correlated output patterning at the level of mitral cell networks<sup>30</sup>. Irrespective of the cellular mechanisms underlying this glomerular phenomenon, the network-based regulation of this mitral cell property appears fundamental to the organization and function of olfactory bulb circuits.

## METHODS SUMMARY

Whole-cell recordings using standard intracellular and extracellular solution were carried out in horizontal olfactory bulb slices (300- $\mu$ m thick) prepared from wild-type C57Bl/6j and M71 transgenic or control littermate mice aged 4–6 weeks. The  $I_h$  current and  $I_h$ -mediated sag potential has recently been extensively characterized for mitral cells<sup>6</sup>, and the details of the experimental and analytical procedures are provided in the Supplementary Information.

Received 7 August 2011; accepted 7 June 2012.

Published online 22 July 2012.

- Gupta, A., Wang, Y. & Markram, H. Organizing principles for a diversity of GABAergic interneurons and synapses in the neocortex. *Science* **287**, 273–278 (2000).
- Brochtrup, A. & Hummel, T. Olfactory map formation in the *Drosophila* brain: genetic specificity and neuronal variability. *Curr. Opin. Neurobiol.* **21**, 85–92 (2011).
- Reyes, A. *et al.* Target-cell specific facilitation and depression in neocortical networks. *Nature Neurosci.* **1**, 279–285 (1998).
- Jinno, S. *et al.* Neuronal diversity in GABAergic long-range projections from the hippocampus. *J. Neurosci.* **27**, 8790–8804 (2007).
- Brown, S. P. & Hestrin, S. Intracortical circuits of pyramidal neurons reflect their long-range axonal targets. *Nature* **457**, 1133–1136 (2009).
- Angelo, K. & Margrie, T. W. Population diversity and function of hyperpolarization-activated current in olfactory bulb mitral cells. *Scientific Reports* **1**, 1:50 (2011).

- Fleischmann, A. *et al.* Mice with a “monoclonal nose”: perturbations in an olfactory map impair odor discrimination. *Neuron* **60**, 1068–1081 (2008).
- Tsiola, A., Hamzei-Sichani, F., Peterlin, Z. & Yuste, R. Quantitative morphologic classification of layer 5 neurons from mouse primary visual cortex. *J. Comp. Neurol.* **461**, 415–428 (2003).
- Schulz, D. J., Goillard, J. M. & Marder, E. Variable channel expression in identified single and electrically coupled neurons in different animals. *Nature Neurosci.* **9**, 356–362 (2006).
- Ermentrout, G. B., Galan, R. F. & Urban, N. N. Reliability, synchrony and noise. *Trends Neurosci.* **31**, 428–434 (2008).
- Marder, E. & Goaillard, J. M. Variability, compensation and homeostasis in neuron and network function. *Nature Rev. Neurosci.* **7**, 563–574 (2006).
- Magee, J. C. Dendritic hyperpolarization-activated currents modify the integrative properties of hippocampal CA1 pyramidal neurons. *J. Neurosci.* **18**, 7613–7624 (1998).
- Garden, D. L., Dodson, P. D., O'Donnell, C., White, M. D. & Nolan, M. F. Tuning of synaptic integration in the medial entorhinal cortex to the organization of grid cell firing fields. *Neuron* **60**, 875–889 (2008).
- George, M. S., Abbott, L. F. & Siegelbaum, S. A. HCN hyperpolarization-activated cation channels inhibit EPSPs by interactions with M-type  $K^+$  channels. *Nature Neurosci.* **12**, 577–584 (2009).
- Nolan, M. F., Dudman, J. T., Dodson, P. D. & Santoro, B. HCN1 channels control resting and active integrative properties of stellate cells from layer II of the entorhinal cortex. *J. Neurosci.* **27**, 12440–12451 (2007).
- Lüthi, A. & McCormick, D. A. Periodicity of thalamic synchronized oscillations: the role of  $Ca^{2+}$ -mediated upregulation of  $I_h$ . *Neuron* **20**, 553–563 (1998).
- Giocomo, L. M., Zilli, E. A., Fransen, E. & Hasselmo, M. E. Temporal frequency of subthreshold oscillations scales with entorhinal grid cell field spacing. *Science* **315**, 1719–1722 (2007).
- Migliore, M. & Shepherd, G. M. Emerging rules for the distributions of active dendritic conductances. *Nature Rev. Neurosci.* **3**, 362–370 (2002).
- Woolsey, T. A. & Van der Loos, H. The structural organization of layer IV in the somatosensory region (SI) of mouse cerebral cortex. The description of a cortical field composed of discrete cytoarchitectonic units. *Brain Res.* **17**, 205–242 (1970).
- Mombaerts, P. Targeting olfaction. *Curr. Opin. Neurobiol.* **6**, 481–486 (1996).
- Schoppa, N. E. & Westbrook, G. L. Glomerulus-specific synchronization of mitral cells in the olfactory bulb. *Neuron* **31**, 639–651 (2001).
- Pimentel, D. O. & Margrie, T. W. Glutamatergic transmission and plasticity between olfactory bulb mitral cells. *J. Physiol.* **586**, 2107–2119 (2008).
- Robinson, R. B. & Siegelbaum, S. A. Hyperpolarization-activated cation currents: from molecules to physiological function. *Annu. Rev. Physiol.* **65**, 453–480 (2003).
- Notomi, T. & Shigemoto, R. Immunohistochemical localization of  $I_h$  channel subunits, HCN1–4, in the rat brain. *J. Comp. Neurol.* **471**, 241–276 (2004).
- Santoro, B. *et al.* Molecular and functional heterogeneity of hyperpolarization-activated pacemaker channels in the mouse CNS. *J. Neurosci.* **20**, 5264–5275 (2000).
- Cadetti, L. & Belluzzi, O. Hyperpolarisation-activated current in glomerular cells of the rat olfactory bulb. *Neuroreport* **12**, 3117–3120 (2001).
- van Welie, I., van Hooft, J. A. & Wadman, W. J. Homeostatic scaling of neuronal excitability by synaptic modulation of somatic hyperpolarization-activated  $I_h$  channels. *Proc. Natl Acad. Sci. USA* **101**, 5123–5128 (2004).
- Desai, N. S., Rutherford, L. C. & Turrigiano, G. G. Plasticity in the intrinsic excitability of cortical pyramidal neurons. *Nature Neurosci.* **2**, 515–520 (1999).
- Padmanabhan, K. & Urban, N. N. Intrinsic biophysical diversity decorrelates neuronal firing while increasing information content. *Nature Neurosci.* **13**, 1276–1282 (2010).
- Dhawale, A. K., Hagiwara, A., Bhalla, U. S., Murthy, V. N. & Albeanu, D. F. Non-redundant odor coding by sister mitral cells revealed by light addressable glomeruli in the mouse. *Nature Neurosci.* **13**, 1404–1412 (2010).

**Supplementary Information** is linked to the online version of the paper at [www.nature.com/nature](http://www.nature.com/nature).

**Acknowledgements** We thank M. Velez-Fort for comments on the manuscript. E.A.R. is a recipient of a Sir Henry Wellcome Fellowship. This project was supported by the Oton Foundation, the Danish Council for Independent Research and the Lundbeckfondation (K.A.), the Gulbenkian PhD Programme and Fundação para a Ciência e Tecnologia (D.P.), The Wellcome Trust (T.W.M.) and Medical Research Council MC\_U1175975156 (B.P. and T.W.M.).

**Author Contributions** K.A. and E.A.R. performed electrophysiological experiments. C.H. and J.H. carried out immunohistochemistry. D.P. performed morphological reconstructions and some initial electrophysiological experiments. B.P. and E.A.R. contributed to data analysis. A.F. generated the transgenic mouse line. K.A. and T.W.M. conceived the project and performed analysis. T.W.M. wrote the paper with input from all other authors.

**Author Information** Reprints and permissions information is available at [www.nature.com/reprints](http://www.nature.com/reprints). The authors declare no competing financial interests. Readers are welcome to comment on the online version of this article at [www.nature.com/nature](http://www.nature.com/nature). Correspondence and requests for materials should be addressed to T.W.M. ([troy.margrie@nimr.mrc.ac.uk](mailto:troy.margrie@nimr.mrc.ac.uk)).